Investigation of long-range sound propagation in surface ducts*

Duan Rui(段 睿), Yang Kun-De(杨坤德)†, and Ma Yuan-Liang(马远良)

Institute of Acoustic Engineering, Northwestern Polytechnical University, Xi'an 710072, *China*

(Received 20 January 2013; revised manuscript received 11 March 2013)

Understanding the effect of source-receiver geometry on sound propagation in surface ducts can improve the performance of near-surface sonar in deep water. The Lloyd-mirror and normal mode theories are used to analyze the features of surface-duct propagation in this paper. Firstly, according to the Lloyd-mirror theory, a shallow point source generates directional lobes, whose grazing angles are determined by the source depth and frequency. By assuming a part of the first lobe to be just trapped in the surface duct, a method to calculate the minimum cutoff frequency (MCF) is obtained. The presented method is source depth dependent and thus is helpful for determining the working depth for sonar. Secondly, it is found that under certain environments there exists a layer of low transmission loss (TL) in the surface duct, whose thickness is related to the source geometry and can be calculated by the Lloyd-mirror method. The receiver should be placed in this layer to minimize the TL. Finally, the arrival angle on a vertical linear array (VLA) in the surface duct is analyzed based on normal mode theory, which provides *a priori* knowledge of the beam direction of passive sonar.

Keywords: surface duct, source-receiver geometry, Lloyd-mirror, normal mode

PACS: 43.30.Cq, 43.30.Bp **DOI:** 10.1088/1674-1056/22/12/124301

1. Introduction

Long-range sound propagation has been an important topic in recent years. The long-range ocean acoustic propagation experiment (LOAPEX),[1] conducted in the northeastern Pacific Ocean, gives rise to many studies on long-range propagation.[2,3] The surface duct is also an effective sound channel for long-range propagation; it differs from the deep ocean channel in its spatiotemporal variability[4] and thus the performance of the near-surface sonar systems may be affected by this duct to different extents for different times and areas. The features of this duct and the sound propagation in it were studied in a previous work. Baker[5]and Schulkin[6] summarized the empirical equations for the transmission loss (TL) of surface-duct propagation at short range based on the experimental data. Labianca[7] and Murphy and Davis[8] described the features of the energy leakage based on normal modes and ray theory, respectively. Porter and Jensen[9] illustrated the importance of leakage with numerical calculations and experimental data. Porter *et al.*[10] introduced the oceanographic and acoustic characteristics of surface ducts. A parameter study was done to indicate the features of surface-duct propagation. This paper is also devoted to a parameter study of the surface duct but the aim is to present explicit expressions for describing the effects of the geometry parameters of sonar[11,12] on its performance. As the requirement for the detection range of the sonar system increases, the working frequency decreases. As is well known, there is a lower bound frequency, called the minimum cutoff frequency (MCF), below which little energy can propagate in the surface duct. However, the previous MCF expression is only for a rough estimation of this lower bound frequency without consideration of the source depth. Since the surface ship sonar, active/passive sonobuoys and dipping sonar work near the ocean surface, the working depth is an important issue when the surface duct exists. In this paper, applying the Lloyd-mirror interference pattern, a new MCF expression is obtained, in which the source depth is taken into account. The new expression gives a simple insight into the appropriate depth to deploy the sonar. Another important issue for the near-surface passive sonar is the optimum depth for receiving signals in the surface duct. It has been known that for the cross-layer source-receiver geometry, the TL is large. For the in-layer source-receiver geometry, the transmission loss can also be large under a certain condition. In this paper, the appropriate receiver depth is presented to obtain low transmission loss.

The array technique is widely used by the sonar system to increase the spatial gain.[13] A prior knowledge of the arrival angle of the signal on the array is beneficial to the good performance.[14] Of course, the arrival angle is related to the source-array geometry and the ocean environment, thus it cannot be determined beforehand. However, for the in-layer source-receiver geometry, the rough arrival angle can be estimated. The detailed theory and simulations based on the normal mode representation are presented in this paper. The normal mode program KRAKEN[15] is used to calculate the TL and the mode.

*Project supported by the National Natural Science Foundation of China (Grant No. 11174235), the Science and Technology Development Project of Shaanxi Province, China (Grant No. 2010KJXX-02), the Science and Technology Innovation Foundation of Northwestern Polytechnical University of China, and the Doctorate Foundation of Northwestern Polytechnical University, China (Grant No. CX201226).

†Corresponding author. E-mail: ykdzym@nwpu.edu.cn

© 2013 Chinese Physical Society and IOP Publishing Ltd

The remainder of this paper is divided into three sections. In Section 2, the theoretical model for the above-mentioned issues is described. In Section 3, the simulations and simple expressions giving insight into the appropriate source-receiver geometry are presented. Besides, the arrival angle on a vertical linear array (VLA) is analyzed based on the normal mode expansion. In Section 4, the findings, including the useful conclusions, are summarized.

2. Theoretical model

The acoustic field can be explained both by the ray theory and the normal mode theory. The two methods are used to investigate different properties of sound propagation in the surface duct.

2.1. Lloyd mirror and MCF

In a deep homogeneous medium, the sound field created by a point source near a smooth, perfectly reflecting sea surface can be calculated by the Lloyd-mirror method. The geometry is shown in Fig. 1. S and S' denote the point source and the image of the source, respectively. z_s denotes the source depth and R is the distance from the origin to the receiver. The declination angle is denoted by θ.

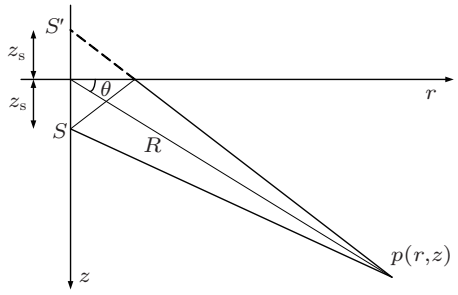


Fig. 1. Geometry for the sound field of a near surface source.

The interference pattern is created by the surface-reflected path and the direct path. The two arrivals add up constructively or destructively and result in high or low acoustic levels. The surface-reflected path appears to be emitted by the image source. Hence, the total sound field can be given by the sum of the two point sources contributions. The detailed derivation can be found in Ref. [16] by Urick. The sound field can be approximated by

$$p(r,z) = 2\left[\frac{zz_s}{R^3}\cos(kz_s\sin\theta) + \mathrm{j}\frac{1}{R}\sin(kz_s\sin\theta)\right]\mathrm{e}^{-\mathrm{j}kR}, \quad (1)$$

where $k = 2\pi/\lambda$ denotes the wavenumber, with λ being the wavelength. In general, $zz_s/R^2 \ll 1$, so the amplitude takes a simple form:

$$|p| = \frac{2}{R}\left|\sin(kz_s\sin\theta)\right|. \quad (2)$$

As the declination angle θ changes from 0 to 90, a directional interference pattern is formed and the directions with maximum and minimum values are given by

$$\sin\theta^m_{\max} = (2m-1)\frac{\pi}{2kz_s}, \quad m = 1,2,\ldots, \quad (3)$$

$$\sin\theta^m_{\min} = (m-1)\frac{\pi}{kz_s}, \quad m = 1,2,\ldots, \quad (4)$$

where $\theta^m_{\max}$ and $\theta^m_{\min}$ denote the directions of the m-th beams with the maximum and the minimum amplitudes, respectively. A typical interference pattern calculated by the Kraken normal mode program is shown in Fig. 2(a) with the sound speed 1500 m/s, the source depth 10 m, and the frequency 1 kHz. Three straight lobes with high intensity (constructive interference) appear to originate from the origin. It seems as if a directional source was placed at the origin.

For an inhomogeneous ocean, the virtual directional source is still a good approximation if the source depth is sufficiently shallow. An ideal example is shown in Fig. 2(b), where the depth and the frequency of the source are also 10 m and 1 kHz, respectively. The sound speed has a constant positive gradient 0.01667 s^{-1} from 1500 m/s at the surface to 1550 m/s at the bottom. Comparing with the propagation in the homogeneous medium (Fig. 2(a)), the first three lobes propagate upward-refracting and thus avoid interacting with the bottom. These lobes propagate at long ranges. Jensen *et al.*[17] have analyzed the properties of the propagation in the Arctic ocean where the sound-speed profile could be approximated by two linear segments with positive gradients. It was assumed that the optimum frequency coincided with that in the situation where the first beam of constructive interference just grazed the bottom.

The Lloyd-mirror pattern can be used to analyze the surface-duct propagation when the source is sufficiently shallow. In general, the surface duct is not deep and the thermocline is always beneath the surface duct in the deep ocean. The beams with steep take-off angles would strike the bottom of the surface duct and propagate downward-refracting, so the energy leakage is significant. In general, the depth of the surface duct is around 100 m in winter, so the number of the lobes trapped in the surface duct is very limited. If the take-off angle of the first lobe, which is frequency and source depth dependent, is so steep that most beams in this lobe cannot be trapped in the surface duct, the sound energy in the duct would be rather low. Therefore, there exists a threshold frequency. If the frequency is higher than the threshold frequency, the first lobe tends to be trapped in the duct and the intensity would be high; if the frequency is lower than the threshold frequency, all lobes cannot be refracted in the duct inversely and the intensity is low. In this paper, the MCF is defined as the threshold which is source-depth-dependent.

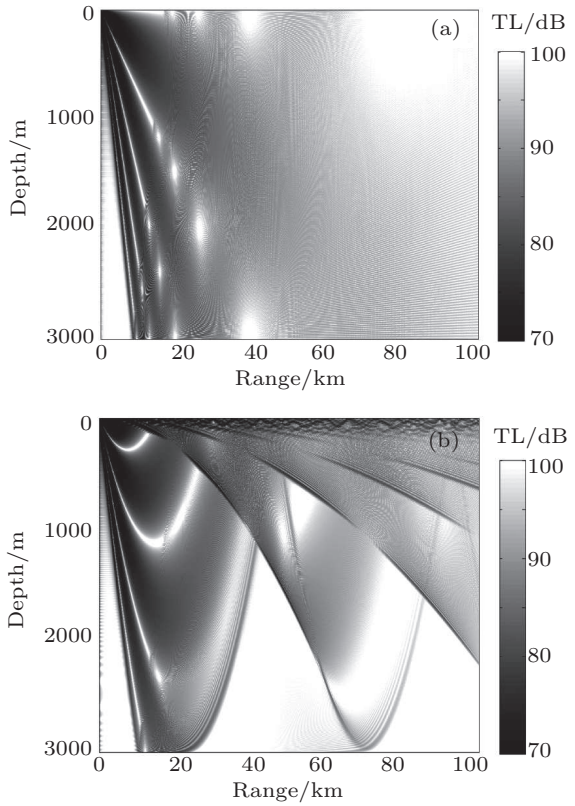


Fig. 2. (a) Lloyd-mirror pattern for homogenous medium. (b) Lloyd-mirror pattern for inhomogeneous medium with positive gradient of sound speed.

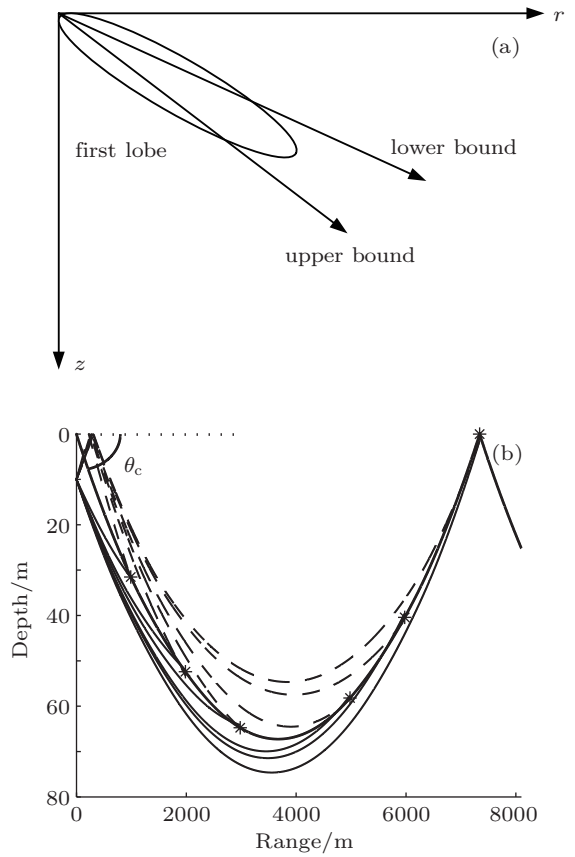


Fig. 3. Schematic illustrations of (a) the boundaries of the first lobe and (b) the critical beam in short range.

In Fig. 3(a), the energy of the first lobe is bounded by two beams whose amplitudes are α times the maximum in the first lobe, where $\alpha < 1$. To determine the MCF, a critical beam is chosen as the lower bound of the first lobe. It is assumed that the MCF coincides with the frequency in the situation where the critical beam is just trapped in the surface duct. The critical beam at short range is the sum of the surface-reflected ray and the direct ray shown in Fig. 3(b). The thick solid line denotes the critical beam. The dashed lines and the thin solid lines denote the surface reflected rays and the direct rays, respectively. The intersections of the rays are marked by the stars. If the critical beam is trapped in the surface duct, the rays that contribute to the beam must be refracted in the duct inversely. It can be seen from Fig. 3(b) that the direct ray that intersects the critical beam at the sea surface has the deepest depth of inverse refraction. The MCF is just the frequency corresponding to this direct ray grazing the bottom of the surface duct.

According to the definition of the critical beam above, the pressure amplitude of the critical beam satisfies

$$p = \alpha p_{\max}, \tag{5}$$

where p is the pressure amplitude of the critical beam and $p_{\max}$ denotes the maximum amplitude in the first lobe. In this paper, α is chosen to be 0.707. Defining the take-off angle from the origin of the critical beam is θ_c; the substitution of the pressure amplitudes in Eq. (2) into Eq. (5) yields

$$kz_s \sin\theta_c = \pi/4. \tag{6}$$

As the sound speed changes little in the surface duct, the wavenumber can be approximated by

$$k = 2\pi f/c_0, \tag{7}$$

where c_0 is the sound speed at the surface.

The take-off angle of the deepest ray can be approximated by θ_c if the source is sufficiently shallow. When the critical beam is just trapped in the surface duct, the deepest ray just grazes the bottom of the surface duct. Therefore, θ_c can be given by Snell's law as follows:

$$c_s/\cos\theta_c = c_{\text{bsd}}, \tag{8}$$

where c_s and c_{bsd} are the sound speeds at the source depth and the bottom of the surface duct, respectively. Combining Eqs. (6), (7) and (8), the MCF is given by

$$f_c = \frac{c_0}{8z_s\sqrt{1-(c_s/c_{\text{bsd}})^2}}, \tag{9}$$

where f_c is the MCF. The lobes cannot be trapped in the surface duct for $f < f_c$ while the first lobe tends to be trapped in

the surface duct for $f > f_c$. As the gradient in the surface duct does not change with depth, a transformation of Eq. (9) is

$$f_c = \frac{c_0(c_0 + gz_d)}{8z_s\sqrt{g(z_d - z_s)(2c_0 + gz_d + gz_s)}}, \tag{10}$$

where g denotes the gradient, z_d the thickness of the surface duct (TSL), and z_s the source depth. In the ocean environment, $c_0 \gg gz_d > gz_s$, so the above expression simplifies into

$$f_c = \frac{1}{8\sqrt{2}} \frac{c_0^{3/2}}{z_s\sqrt{g(z_d - z_s)}}. \tag{11}$$

Assuming that the sound speed of the surface is 1500 m/s and the gradient is 0.01667 m/s, when the source is placed at a quarter of the surface duct near the surface, the MCF from Eq. (11) is

$$f_c = 183700 z_d^{-2/3}, \tag{12}$$

which is consistent with the MCF expression given by Urick.[16] Equation (11) indicates that the MCF is primarily determined by the source depth, the sound speed of the surface, the gradient of the sound speed, and the TSL. Thus a shallower source, smaller thickness or smaller gradient of the surface duct would result in a higher MCF.

2.2. Arrival angle on the VLA in surface duct

According to normal mode theory, for an isotropic point source, the acoustic pressure in far fields can be expressed in terms of normal modes expansion,[17,18]

$$p(r,z;r_s,z_s) = \frac{\mathrm{i}}{\rho(z_s)\sqrt{8\pi(r - r_s)}} \mathrm{e}^{-\mathrm{i}\pi/4} \times \sum_{m=1}^{M} \varphi_m(z_s)\varphi_m(z) \frac{\mathrm{e}^{\mathrm{i}k_m(r - r_s)}}{\sqrt{k_m}}, \tag{13}$$

where the harmonic time dependence of $\exp(-\mathrm{i}\omega t)$ is neglected; the eigenfunction φ_m is the normalized mode function and in the far field, the eigenfunctions are all real; k_m is the corresponding eigenvalue, representing the horizontal wavenumber; M is the number of modes that contribute to the far field; (r_s, z_s) and (r, z) are the source position and the receiver position in the cylindrical coordinates, respectively. The data vector received on a VLA at range r is

$$\boldsymbol{x} = [p(r,z_1;r_s,z_s), p(r,z_2;r_s,z_s), \ldots, p(r,z_N;r_s,z_s)]^{\mathrm{T}}, \tag{14}$$

where N denotes the number of elements, $\boldsymbol{x}$ is the data vector and z_i is the depth for the i-th element.

The beamforming output of the VLA is

$$y = \boldsymbol{w}(\theta)^{\mathrm{H}}\boldsymbol{x}, \tag{15}$$

where the $(\,)^{\mathrm{H}}$ denotes conjugate transpose, $\boldsymbol{w}(\theta)$ is the steering vector and is expressed as,

$$\boldsymbol{w}(\theta) = [1, \mathrm{e}^{\mathrm{i}kd\sin\theta}, \mathrm{e}^{\mathrm{i}k2d\sin\theta}, \ldots, \mathrm{e}^{\mathrm{i}k(N-1)d\sin\theta}]^{\mathrm{T}}, \tag{16}$$

with k being the wavenumber of the signal, d the spacing between elements and θ the steering angle. Changing the steering angle from -90° to 90°, the power output of the conventional beamformer is then given by

$$P(\theta) = y * y^{\mathrm{H}} = \boldsymbol{w}(\theta)^{\mathrm{H}}\boldsymbol{x} * \boldsymbol{x}^{\mathrm{H}}\boldsymbol{w}(\theta). \tag{17}$$

Substituting Eqs. (13) and (14) into Eq. (15) and assuming r_s to be equal to zero for simplicity, one obtains

$$y(\theta) = \frac{\mathrm{i}}{\rho(z_s)\sqrt{8\pi r}} \mathrm{e}^{-i\pi/4} \times \boldsymbol{w}(\theta)^{\mathrm{H}} \cdot \begin{bmatrix} \sum_{m=1}^{M} \varphi_m(z_s)\varphi_m(z_1) \frac{\mathrm{e}^{\mathrm{i}k_m(r)}}{\sqrt{k_m}} \\ \sum_{m=1}^{M} \varphi_m(z_s)\varphi_m(z_2) \frac{\mathrm{e}^{\mathrm{i}k_m(r)}}{\sqrt{k_m}} \\ \cdots \\ \sum_{m=1}^{M} \varphi_m(z_s)\varphi_m(z_N) \frac{\mathrm{e}^{\mathrm{i}k_m(r)}}{\sqrt{k_m}} \end{bmatrix}. \tag{18}$$

Using the notations

$$\Psi_m = [\varphi_m(z_1), \varphi_m(z_2), \ldots, \varphi_m(z_N)]^{\mathrm{T}}, \tag{19}$$

$$A_m = \frac{i}{\rho(z_s)\sqrt{8\pi r}} \mathrm{e}^{-i\pi/4} \varphi_m(z_s) \frac{\mathrm{e}^{\mathrm{i}k_m(r)}}{\sqrt{k_m}}, \tag{20}$$

equation (18) becomes

$$y = \sum_{m=1}^{M} A_m \boldsymbol{w}(\theta)^{\mathrm{H}}\Psi_m, \tag{21}$$

where Ψ_m is the spatial sampling of the m-th mode and A_m is the amplitude of the m-th mode. Substituting Eq. (21) into Eq. (17), one obtains

$$P(\theta) = \sum_{i=1}^{M}\sum_{j=1}^{M} A_i A_j^{\mathrm{H}} \boldsymbol{w}(\theta)^{\mathrm{H}}\Psi_i\Psi_j^{\mathrm{H}}\boldsymbol{w}(\theta). \tag{22}$$

Equation (22) can be expressed as the sum of two parts, i.e.,

$$P(\theta) = \sum_{i=1}^{M} A_i A_i^{\mathrm{H}} \boldsymbol{w}(\theta)^{\mathrm{H}}\Psi_i\Psi_i^{\mathrm{H}}\boldsymbol{w}(\theta) + \sum_{i=1}^{M}\sum_{j=1, i\neq j}^{M} A_i A_j^{\mathrm{H}} \boldsymbol{w}(\theta)^{\mathrm{H}}\Psi_i\Psi_j^{\mathrm{H}}\boldsymbol{w}(\theta), \tag{23}$$

where the first part is the sum of the array responses to each mode. The second part is the coupled effects of the modes on the array. From Eq. (20), one obtains

$$A_i A_j^{\mathrm{H}} = \begin{cases} \dfrac{\varphi_i^2(z_s)}{8\pi\rho^2(z_s)rk_i}, & i = j, \\ \dfrac{\varphi_i(z_s)\varphi_j(z_s)}{8\pi\rho^2(z_s)r\sqrt{k_i k_j}} \mathrm{e}^{\mathrm{i}(k_i - k_j)r}, & i \neq j. \end{cases} \tag{24}$$

As shown in Eq. (24), when $i = j$, the real coefficient $A_i A_i^{\mathrm{H}}$ only contains a variable term of $1/r$, which does not contribute to the arrival angle. However, when $i \neq j$, the complex coefficients $A_i A_j^{\mathrm{H}}$ and $A_j A_i^{\mathrm{H}}$ each involve an oscillatory term of the form $\mathrm{e}^{\pm \mathrm{i}(k_i - k_j)r}$, which indicates that the arrival angle oscillates around the value associated with the first term of Eq. (23). The two terms can be combined into one oscillatory term $T_{i,j}$,

$$T_{i,j} = C_{i,j}\cos((k_i - k_j)r + \varphi_{i,j}), \tag{25}$$

where $C_{i,j}$ is the amplitude of the oscillatory term and is given by

$$C_{i,j} = 2\frac{\varphi_i(z_{\mathrm{s}})\varphi_j(z_{\mathrm{s}})}{8\pi\rho^2(z_{\mathrm{s}})r\sqrt{k_i k_j}}\left|\boldsymbol{w}(\theta)^{\mathrm{H}}\Psi_i\Psi_j^{\mathrm{H}}\boldsymbol{w}(\theta)\right|, \tag{26}$$

and $\varphi_{i,j}$ is the phase of the oscillatory term and can be expressed as

$$\varphi_{i,j} = \arctan\left(\frac{\mathrm{imag}(\boldsymbol{w}(\theta)^{\mathrm{H}}\Psi_i\Psi_j^{\mathrm{H}}\boldsymbol{w}(\theta))}{\mathrm{real}(\boldsymbol{w}(\theta)^{\mathrm{H}}\Psi_i\Psi_j^{\mathrm{H}}\boldsymbol{w}(\theta))}\right). \tag{27}$$

Equation (23) becomes

$$P(\theta) = \sum_{i=1}^{M}\frac{\varphi_i^2(z_{\mathrm{s}})}{8\pi\rho^2(z_{\mathrm{s}})rk_i}\boldsymbol{w}(\theta)^{\mathrm{H}}\Psi_i\Psi_i^{\mathrm{H}}\boldsymbol{w}(\theta) + \sum_{i=1}^{M-1}\sum_{j=i+1}^{M}C_{i,j}\cos((k_i - k_j)r + \varphi_{i,j}). \tag{28}$$

The first part on the right-hand side of Eq. (28) denotes the mean arrival angle and the second part refers to the oscillatory term. The contributions of normal modes to the arrival angle are $\varphi_i(z_{\mathrm{s}})$ dependent and thus the modes with large amplitudes at the source depth are dominant. As will be seen in Section 4, these dominant modes play a primary role in both the mean term and the oscillatory term of the arrival angle.

The oscillatory cycles of the arrival angle in terms of range can be estimated by

$$R_{i,j} = 2\pi/\left|k_i - k_j\right|, \tag{29}$$

where $R_{i,j}$ is the range cycle corresponding to the i-th and the j-th modes; k_i and k_j are the horizontal wavenumbers of the i-th and j-th modes, respectively.

3. Transmission loss in the surface duct

3.1. MCF and source depth

To illustrate the features of sound propagation in the surface duct, simulations are performed in a typical deep-water environment, as shown in Fig. 4. The TSL is 112 m. The bottom is represented by an infinite halfspace. The sound speed and the density of the bottom are 1600 m/s and 1600 kg/m^3, respectively. As we focus on the sound trapped in the surface duct, the attenuation of sound in the bottom is 8 dB/m. Under this condition, the bottom-reflected rays are highly lossy and have small effects on the sound field in the surface duct, especially for the long-range propagation.

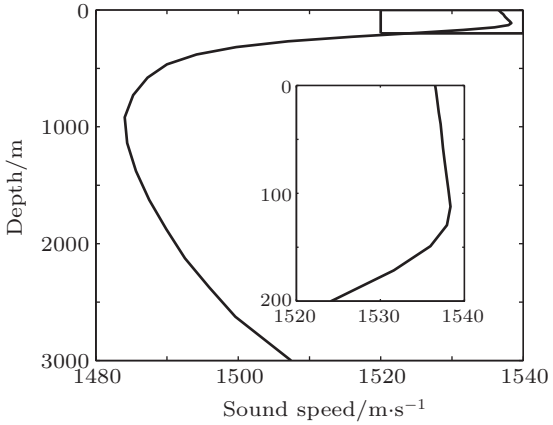


Fig. 4. Sound speed profile in the deep-water environment.

Two typical surface-duct propagations with 10-m sources in the deep-water environment are shown in Figs. 5(a) and 5(b), where the frequencies are 300 Hz and 500 Hz, respectively. The MCF determined by Eq. (9) is 414 Hz. The vertical lobe near 20 km is the bottom-reflected rays. TheTL for a 500-Hz source is about 10-dB lower than that for 300 Hz in the surface duct, which demonstrates that when the source depth is 10 m, the 112-m surface duct is effective in trapping sound with a frequency above 400 Hz. Different propagations occur when the source depth changes. When the source depth is 20 m and the frequency is 300 Hz, the propagation is as shown in Fig. 5(c). When the source depth is 4 m and the frequency is 500 Hz, the propagation is as shown in Fig. 5(d). When the source depths are 20 m and 4 m, the MCFs calculated from Eq. (9) are 218 Hz and 1005 Hz, respectively. A comparison between Fig. 5(a) and Fig. 5(c) shows that although the frequencies are the same, the difference between their TLs is about 10 dB. The same phenomenon is shown in Figs. 5(b) and 5(d). It can be concluded from the above comparison that the source depth has a significant effect on TL. The MCF expressed by Eq. (9) gives a reasonable lower frequency bound of the sound trapped in the surface duct.

The minimum TL in a surface duct at 100 km versus the source depth and frequency is shown in Fig. 6, where the MCF from Eq. (9) is shown by the solid line. Some points can be drawn from Fig. 6. First, when the source is near the surface, the MCF decreases with increasing source depth. It is shown by the pattern marked by the rectangle in Fig. 6. When the source is near the surface within 3 m, the TL is very high. Second, when the source is placed near the bottom of the surface duct, the TL increases with increasing source depth, which is shown by the pattern where the source is deeper than 90 m. Third, when the frequency is above 1500 Hz, the TL increases fast; it is because of the sea-water attenuation.

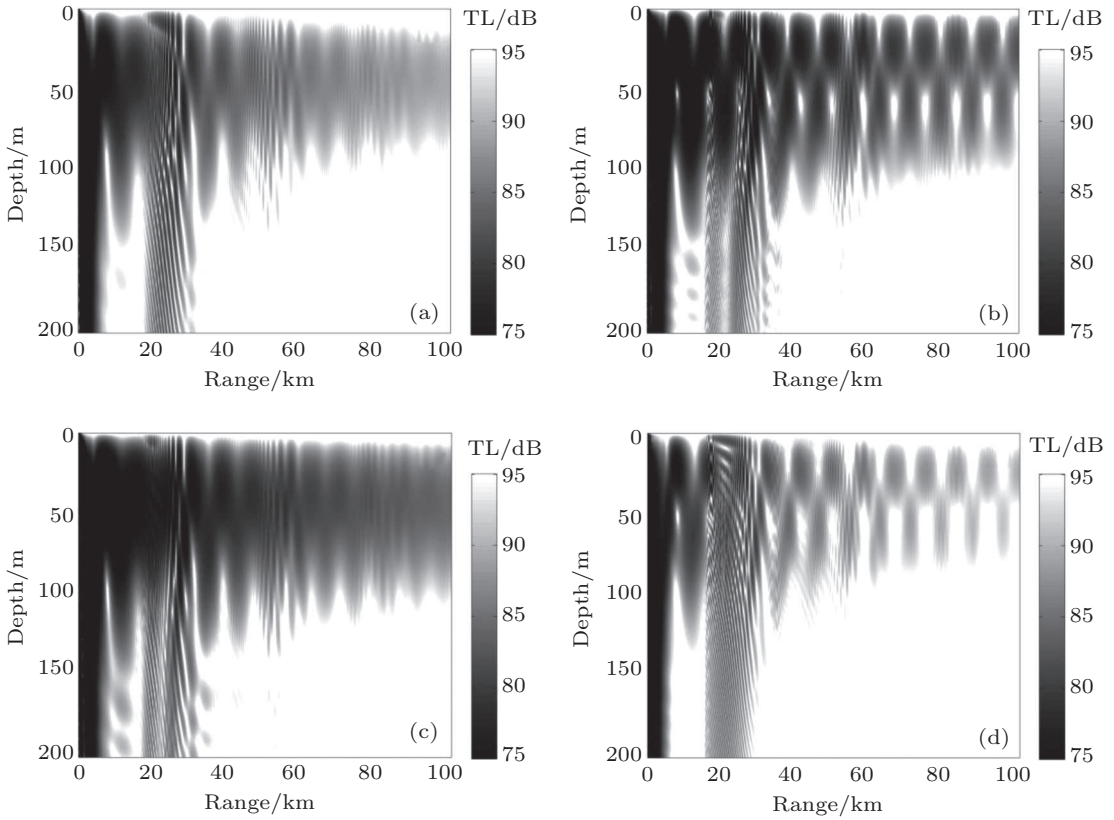


Fig. 5. TLs of the surface-duct propagations with different source depths and frequencies: (a) 10 m and 300 Hz, (b) 10 m and 500 Hz, (c) 20 m and 300 Hz, (d) 4 m and 500 Hz.

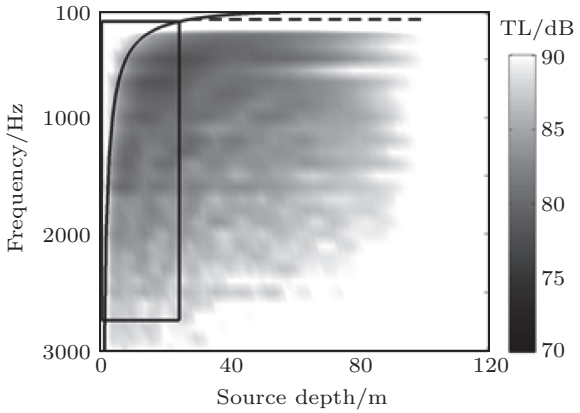


Fig. 6. Minimum TL at 100 km versus source depth and frequency. The TSL is 112 m.

Figure 6 shows that the simulated MCF changes with the source depth and accords well with the MCF from Eq. (9) for shallow source depths within the rectangle. However, when the source is deeper, the MCF from Eq. (9) is lower than the simulated result. This is because the Lloyd-mirror method is valid under a shallow source. A combined MCF can be given by

$$f_{\mathrm{c}} = \begin{cases} \dfrac{1}{8\sqrt{2}} \dfrac{c_0^{3/2}}{z_{\mathrm{s}}\sqrt{g(z_{\mathrm{d}}-z_{\mathrm{s}})}}, & z_{\mathrm{s}} \le z_{\mathrm{d}}/4, \\ \dfrac{1}{\sqrt{6g}} \left(\dfrac{c_0}{z_{\mathrm{d}}}\right)^{3/2}, & z_{\mathrm{s}} > z_{\mathrm{d}}/4, \end{cases} \tag{30}$$

where the second equation is obtained by setting the source depth to be quarter of the TSL and accords well with the expression of the MCF given by Urick.[16] The MCF from Eq. (30) is shown by the dashed line in Fig. 6.

The pattern when the source is deeper than 90 m can be explained by the ray theory. The angle range of the trapped rays increases with the increase of the spacing between the source and the bottom of the surface duct. If the spacing is small, the angle range of rays trapped in the duct is rather small. All the rays that contribute to the interference pattern at short range have steep take-off angles and thus cannot be trapped in the duct. Thus, the interference pattern can only be found at a very short range and the lobes cannot propagate to a long range. The lower bound of the source depth estimated from Fig. 6 is about 20 m shallower than the bottom of the surface duct. This conclusion also holds true for the surface ducts with different thickness values. The minimum TL calculations at 100 km with the TSLs of 46 m and 83 m are shown in Figs. 7(a) and 7(b), respectively. Figure 7 shows the same phenomenon as Fig. 6, that is, when the source is near the surface, the MCF will increase with source depth decreasing. A comparison between Fig. 7(a) and Fig. 7(b) shows that the MCF significantly increases with TSL increasing.

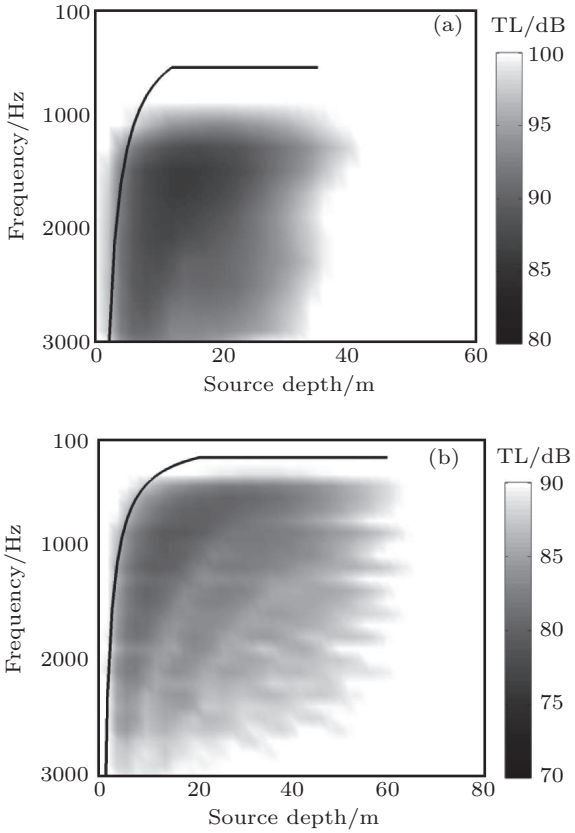


Fig. 7. Minimum TLs at 100 km versus source depth and frequency with TSLs being (a) 46 m and (b) 83 m.

In a word, for a fixed frequency, the source should be placed between two depths. One is the depth where the MCF from Eq. (30) equals the frequency. The other one is 20 m shallower than the bottom of the surface duct.

3.2. Receiver depth

As demonstrated in Subsection 2.1, the take-off angles of the lobes are dependent on the source depth and source frequency. When the take-off angles are small enough, the lobes are trapped in the surface duct. Supposing that the source depth is constant and the frequency is above the MCF, the take-off angle of the first lobe would decrease with frequency increasing and this lobe would be refracted within a near-surface layer. Therefore, before the second lobe is trapped in the surface duct, the thickness of the layer of low TL (low-loss layer) in the surface duct decreases with frequency increasing. The changing process is shown in Fig. 8, where the source depth is 20 m. The frequencies are 400 Hz in Fig. 8(a) and 1000 Hz in Fig. 8(b). The thickness of the low-loss layer in Fig. 8(b) is apparently smaller than that in Fig. 8(a). As a result, the receiver below 60 m receives a weak signal. The thickness of the layer caused by the first lobe can be calculated by the Lloyd-mirror pattern. Supposing that the first lobe is entirely trapped in the lobe, the thickness of the low-loss layer coincides with the depth at which the second beam of destructive interference is effectively refracted within the duct. The declination angle of this beam is $\theta_{\min}^{m=2}$ calculated by Eq. (4). Therefore, the thickness can be calculated by

$$\frac{c_0}{\cos\theta_{\min}^{m=2}} = c_T, \tag{31}$$

$$c_T = c_0 + gT, \tag{32}$$

where c_T is the sound speed at the bottom of the low-loss layer and T denotes the thickness of this low-loss layer. Finally, T is given by

$$T = \frac{c_0}{g}\left(\frac{1}{\sqrt{1-(c_0/2fz_s)^2}} - 1\right), \tag{33}$$

where f and z_s are the frequency and the depth of the source, respectively. When the frequency is 1000 Hz and the source depth is 20 m, the thickness of the low-loss layer is calculated by Eq. (33) to be 62 m, which accords well with the simulated result shown in Fig. 8(b).

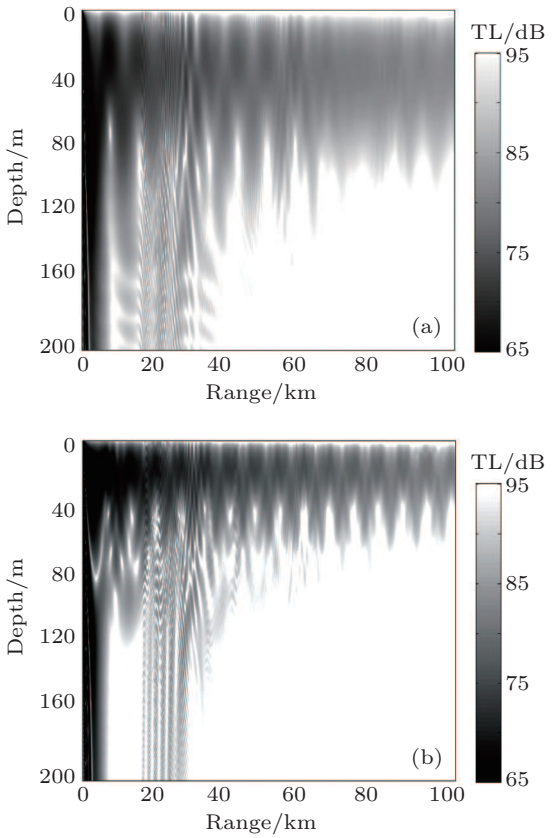


Fig. 8. Variations of TLs of surface duct propagation with range at frequencies of (a) 400 Hz and (b) 1000 Hz when the source depth is 20 m and the TSL is 112 m.

If the frequency is high enough, the second lobe will be refracted in the surface duct and the phenomenon of two low-loss layers is formed. The two-layer pattern is shown in Fig. 9(a), where the source depth is 20 m and the frequency is 1200 Hz. The first layer is within 50 m and is the result of the first lobe, while the second layer is between 50 m and 110 m and represents the propagation of the second lobe. The shadow

zone between the two layers is caused by destructive interference beams. Even when the frequency is higher, the interference pattern in the surface duct is complicated. In Fig. 9(b), the source depth is 20 m and the frequency is 1600 Hz. Although the interferences are complicated, two low-loss layers can also be identified. The depth of the first layer from Eq. (33) is 24 m, which is a good approximation of the simulated result.

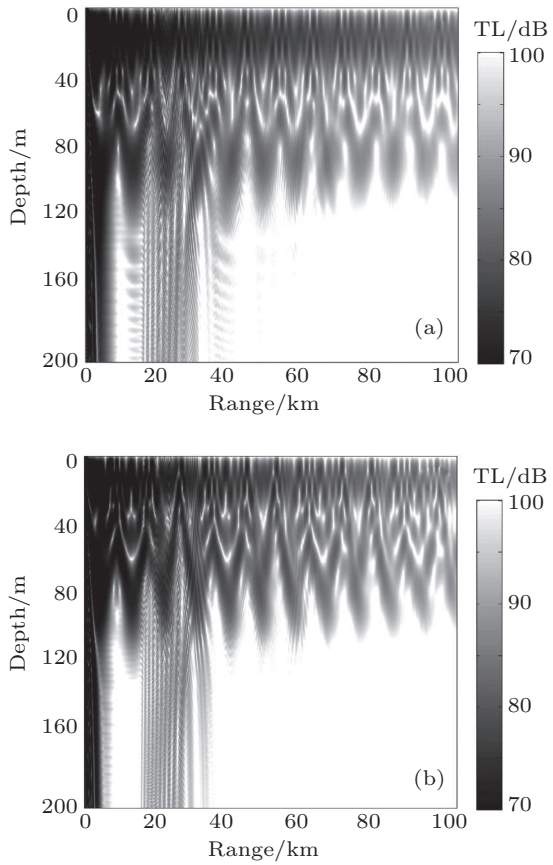


Fig. 9. Variations of TL of surface duct propagation with the range at frequencies of (a) 1200 Hz and (b) 1600 Hz when the source depth is 20 m and the TSL is 112 m.

In conclusion, our analysis shows that an optimum receiver depth exists in surface ducts where the TL in the duct is low. In general, the receiver should not be placed near the bottom of the surface duct where the energy leakage is significant, as shown in Fig. 8(a). If the frequency is above the MCF, there exists a low-loss layer in the surface duct. When the first lobe is entirely trapped in the duct, the thickness of this layer decreases with the frequency increasing. If the frequency is so high that part of the second lobe is refracted within the surface duct, two low-loss layers are formed. There is a shadow zone between the two layers and thus the receiver should not be placed in it.

The sensitivity of the MCF to the feature of the surface duct is concluded here. The following characteristics can be deduced from Eq. (11). First, the MCF is proportional to the 1.5th power of the sound speed at the surface. Second, the MCF is inversely proportional to the square root of the gradient. Third, when the source depth is constant, the MCF increases with TSL decreasing.

4. Simulations of the arrival angle

In this section, the arrival angle derived in Subsection 2.2 and its dependence on the dominant mode are illustrated by simulations. In Subsection 4.1, the arrival angle on a VLA under certain environment and source geometries are presented, where the effects of the dominant modes are shown. In Subsection 4.2, a complete analysis is performed and generalized conclusions are given.

4.1. A typical example

The acoustic environment is shown in Fig. 4. The VLA consists of 101 elements with spacings of 0.5 m. The first element is located at 10 m below the sea's surface. The source depth is 20 m and the frequency is 800 Hz. The modes are solved by the normal mode program KRAKEN.[15] The first term on the right-hand side of Eq. (28) presenting the mean arrival angle is the weighted sum of array responses to the mode. Figures 10(a) and 10(b) show the normalized array responses to each mode and the corresponding weights $\varphi_i(z_s)$, respectively. The dashed line in Fig. 10(a), where the mode number is 727, is a boundary mode below which the mode function keeps near zero in the surface duct. Figure 10(a) shows that as the mode number increases, the maximum output angles are symmetric and deviate gradually from the horizontal direction. Figure 10(b) shows that the majority of modes are very weak compared with the strongest mode and only a few modes defined as dominant modes contribute to Eq. (28). In this paper, the dominant modes are defined as the modes whose amplitudes are lower than the maximum amplitude within 10 dB. Under this environment, there are two dominant modes, as shown in Fig. 10(c). If these two modes are used to calculate Eq. (28), the first term, independent of range, is shown in Fig. 10(d). The VLA has the maximum output at 0. This phenomenon is due to the mode 727 that the spatial samplings of this mode are all positive and thus the energy output is at 0. The second term of Eq. (28) is $T_{1,2}$ and the cycle range is $2\pi/|k_1 - k_2|$, which equals 8.06 km.

The arrival angles versus the range by Eq. (28) using all the modes are shown in Fig. 11(a). The frequency spectrum of the arrival angle is shown in Fig. 11(b), where the frequency is transformed to range for simplicity. Figure 11(a) shows that the arrival angle oscillates around 0 and the oscillatory amplitude, below 2, is very weak. Figure 11(b) shows that the strongest range cycle (SRC) is 8.35 km, which is close to the interference range of the two dominant modes (Fig. 10(c)). These two results are consistent with the effects of the two dominant modes, which illustrates that the arrival angle is determined by the dominant modes in the surface duct.

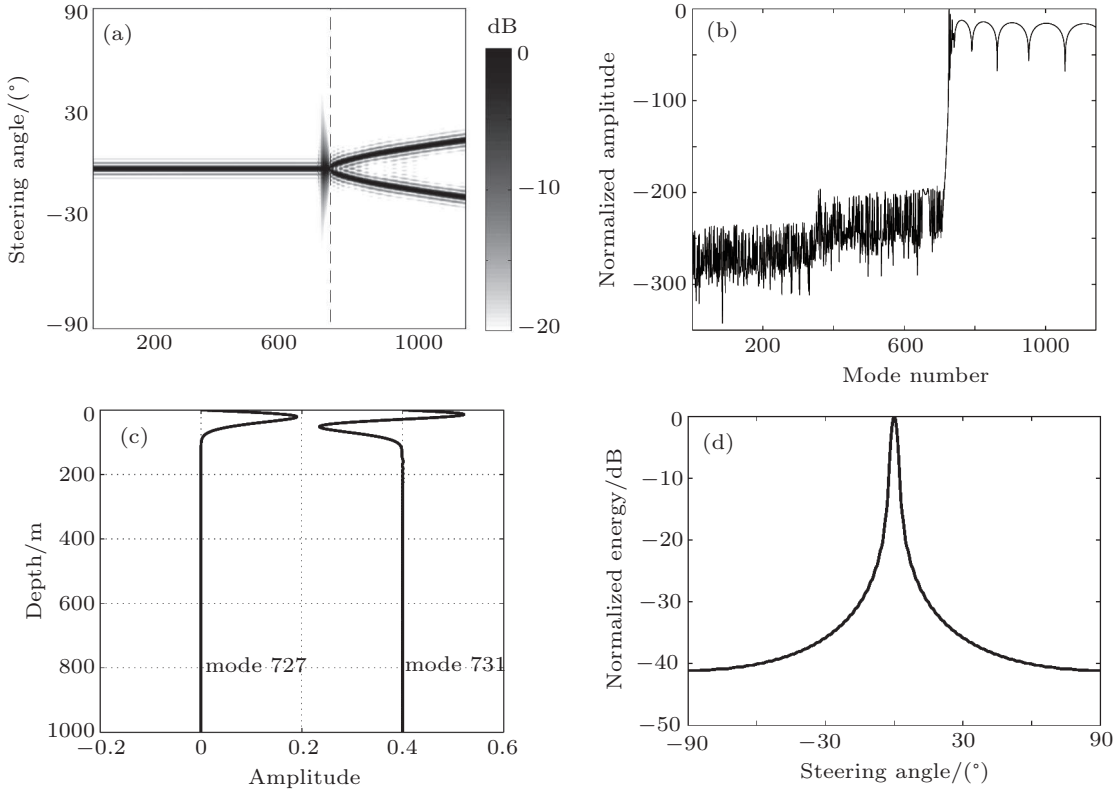


Fig. 10. Features of modes in the surface duct for an 800 Hz source placed at 20 m. (a) Array responses to each mode. (b) Normalized mode amplitudes. (c) Two dominant modes. (d) Array responses to the dominant modes.

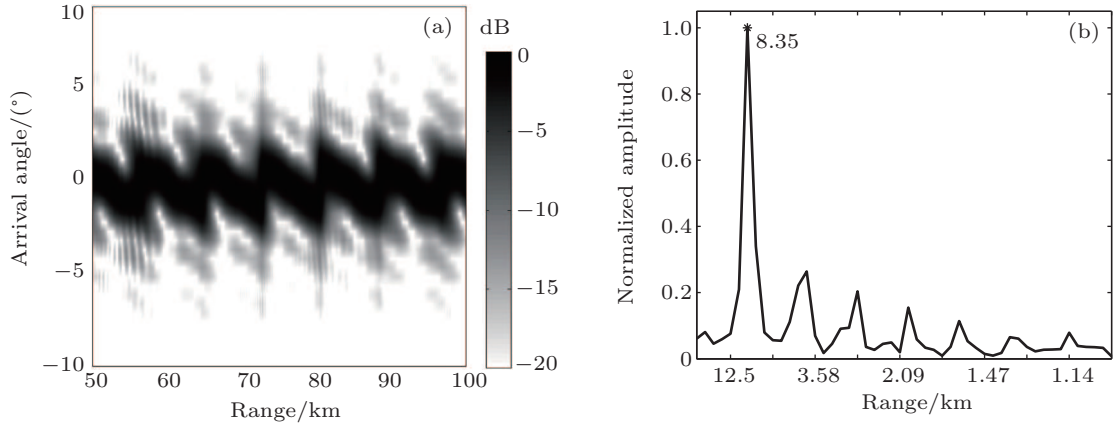


Fig. 11. Features of the arrival angle for an 800 Hz source placed at 20 m. (a) Arrival angle and (b) normalized spectrum versus range.

In general, the dominant modes change with the source depth. However, in the surface duct, the modes with a few zeros in the surface duct are much stronger than the modes with more zeros in the surface duct. For example, the modes 727 and 731, shown in Fig. 10(c), only have one or two zeros in the surface duct. The dominant modes under different source depths are shown in Table 1. Table 1 shows that when the source is placed within one third of the TSL (about 40 m), the strongest mode is mode 727 and thus the mean arrival angle is around 0. When the source is placed closer to the bottom of the surface duct, the number of dominant modes increases and the arrival angles gradually deviate from the horizontal direction.

Table 1. Dominant modes for different source depths.

Source depth/m	Dominant modes	Mean arrival angle/(°)	Source depth/m	Dominant modes	Mean arrival angle/(°)
10	727,731,736,740	0	50	731	±1
20	727	0	70	731,736	±1.6
30	727	0	90	736,739,746	±2.3
40	727,731,736	±0.6	100	736,739,740,744	±2.5

In conclusion, the dominant modes for a source in the surface duct are the ones that have few zeros in the surface duct. As a result, the arrival angles are close to zero. The oscillation of the arrival angle results from the interference effects of the dominant modes; the oscillatory cycles can be estimated by the horizontal wavenumbers of the dominant modes.

4.2. Generalized results

In this section, the conclusions drawn from Subsection 4.1 are generalized to various cases. First, the method of calculating the oscillatory cycle is generalized to the case where more than two dominant modes exist in the surface duct. Second, the mean arrival angles are generalized to the cases of different frequencies based on the analysis of low-order modes.

In general, the oscillatory term in Eq. (28) has many different oscillatory cycles. As the amplitudes of these cycles are different, the strong ones may drown out the weak ones. If the modes are rearranged by sorting their amplitudes at the source depth according to descending order, then substituting the horizontal wavenumbers of the first two modes into Eq. (29), the range cycle of the strongest oscillatory term (RCSOT) can be given by

$$R = 2\pi / |k_1 - k_2| , \tag{34}$$

where k_1 and k_2 are the horizontal wavenumbers of the first two dominant modes. Many simulations are done to verify this generalization. For simplicity, the source depth is shallow and thus the mean arrival angle is 0. The TSL is 112 m. The values of RCSOT and the SRC for various cases are shown in Table 2. The values of RCSOT accord well with those of the SRC and the errors are within 5 percent.

Table 2. Comparisons of RCSOT and the SRC among various cases.

Number	Source depth/m	Frequency/Hz	k_1/m^{-1}	k_2/m^{-1}	RCSOT/km	SRC/km
1	20	400	1.6346	1.6338	8.2834	8.5900
2	20	600	2.4523	2.4514	7.3778	7.5100
3	20	1000	4.0876	4.0866	6.5983	6.6800
4	20	1200	4.9055	4.9024	2.0748	2.0700
5	10	2000	8.1761	8.1748	5.0293	5.0100
6	10	2500	10.2206	10.2191	4.2045	4.2900

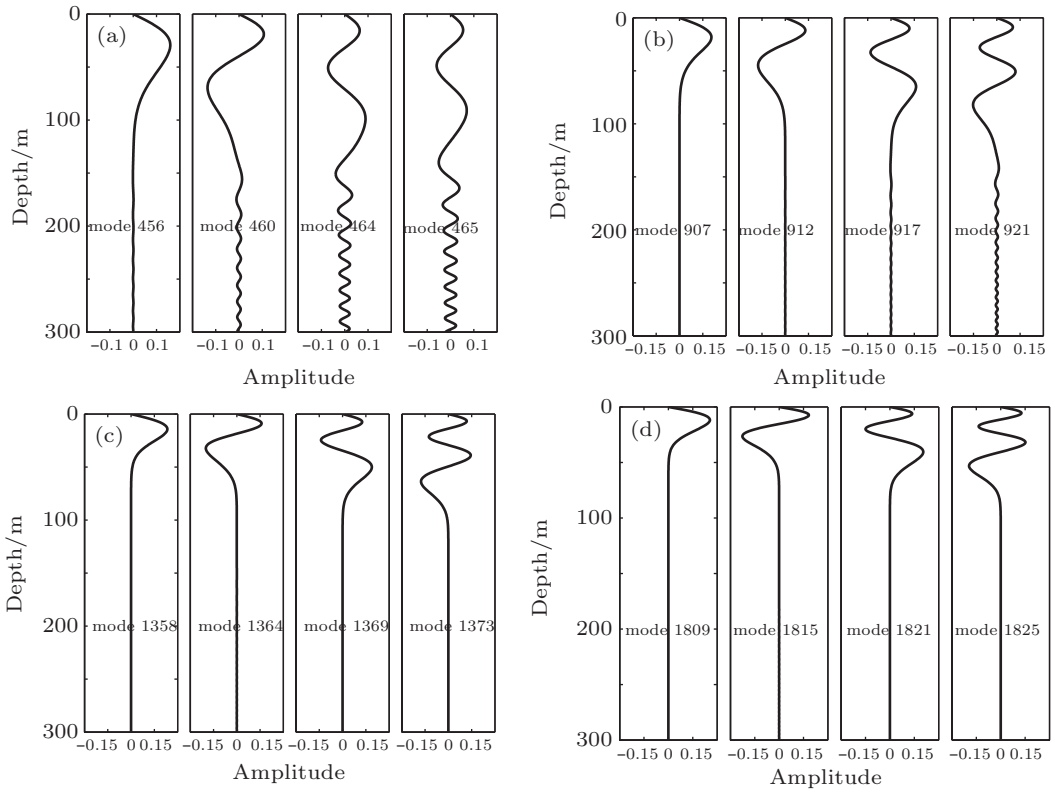


Fig. 12. Low-order modes in the surface duct with frequencies of (a) 500 Hz, (b) 1000 Hz, (c) 1500 Hz, and (d) 2000 Hz.

It is shown in the last section that the dominant modes for a source are the ones that have few zeros in the surface duct. These modes are the low-order modes in terms of the surface duct. When the TSL is 112 m, the low-order modes are given under different frequencies, which are shown in Fig. 12. It is shown in Fig. 12 that the low-order modes for different frequencies are qualitatively similar. Therefore, the mean arrival angles are also close to 0. However, the depth spans for these modes decrease with the frequency increasing. For example, the depth span of the mode 456 under 500 Hz is in a range from 0 m to 100 m while the depth span of the mode 1809 under 2 kHz is in a scope between 0m and 40 m. It indicates that if the source moves towards the surface-duct bottom, the arrival angle will deviate from 0 faster under a higher frequency.

5. Summary and conclusions

Based on the Lloyd-mirror and normal mode theories, the effects of source-receiver geometry on the sound propagation in surface ducts are analyzed. Useful conclusions are summarized as follows.

(i) The MCF is deduced based on the Lloyd-mirror theory. Equation (9) shows the relationship between the MCF and both the characteristics of the surface duct and the source depth. The source depth has a significant effect on the MCF.

(ii) For a fixed frequency, the source should be placed between two depths. One is the depth where the MCF from Eq. (30) equals the source frequency. The other one is 20 m shallower than the bottom of the surface duct.

(iii) The receiver should be placed in the low-loss layer for low TL. The thickness of the low-loss layer can be calculated by Eq. (33), when the first lobe is entirely in the surface duct.

(iv) For a VLA in the surface duct, the arrival angle is close to 0. For deeper source and higher frequency, the deviation from 0 is larger. The oscillation of the arrival angle results from the interference of the dominant modes; the oscillatory cycle can be estimated by the horizontal wavenumbers of the dominant modes.

References

[1] Mercer J A, Howe B M, Andrew R K, Wolfson M A, Worcester P F, Dzieciuch M A and Colosi J A 2006 *J. Acoust. Soc. Am.* **120** 3020

[2] Grigorieva N S, Fridman G M, Mercer J A, Andrew R K, Wolfson M A, Howe B M and Colosi J A 2009 *J. Acoust. Soc. Am.* **125** 1919

[3] Van Uffelen L J, Worcester P F, Dzieciuch M A, Rudnick D L and Colosi J A 2010 *J. Acoust. Soc. Am.* **127** 2169

[4] Duan R, Yang K D, Ma Y L and Hu T 2012 *Acta. Oceanol. Sin.* **31** 19

[5] Baker W F 1975 *J. Acoust. Soc. Am.* **57** 1198

[6] Schulkin M 1968 *J. Acoust. Soc. Am.* **44** 1152

[7] Labianca F M 1973 *J. Acoust. Soc. Am.* **53** 1137

[8] Murphy E L and Davis J A 1974 *J. Acoust. Soc. Am.* **56** 1747

[9] Porter M B and Jensen F B 1993 *J. Acoust. Soc. Am.* **94** 1510

[10] Porter M B, Piacsek S, Henderson L and Jensen F B 1993 *Surface Duct Propagation and the Ocean Mixed Layer* in *Oceanography and Acoustics Prediction and Propagation Models* (New York: AIP)

[11] Ying Y Z, Ma L and Guo S M 2011 *Chin. Phys. B* **20** 054301

[12] Li X G, Yang K D and Wang Y 2011 *Chin. Phys. B* **20** 074301

[13] Zhang T W, Yang K D and Ma Y L 2010 *Chin. Phys. B* **19** 124301

[14] Ma J, Gao C and Tan L Y 2007 *Chin. Phys.* **16** 1327

[15] Porter M B 1992 *The KRAKEN Normal Mode Program*, DTIC Document

[16] Urick R J 1983 *Principles of Underwater Sound*, 3rd edn. (New York: McGraw-Hill)

[17] Jensen F B, Kuperman W A, Porter M B and Schmidt H 1994 *Computational Ocean Acoustics* (New York: AIP)

[18] Wang N and Liu J Z 2002 *Chin. Phys.* **11** 456